

SwinIA: Self-Supervised Blind-Spot Image Denoising with Zero Convolutions

Mikhail Papkov Pavel Chizhov
 Institute of Computer Science, University of Tartu
 Tartu, Estonia
 {mikhail.papkov,pavel.chizhov}@ut.ee

Abstract

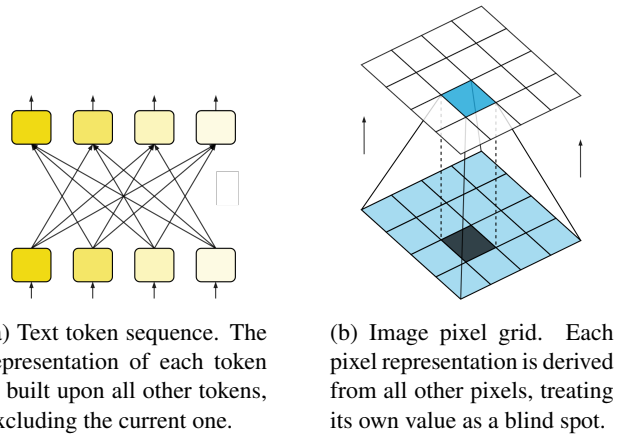
The essence of self-supervised image denoising is to restore the signal from the noisy image alone. State-of-the-art solutions for this task rely on the idea of masking pixels and training a fully-convolutional neural network to impute them. This most often requires multiple forward passes, information about the noise model, and intricate regularization functions. In this paper, we propose a Swin Transformer-based Image Autoencoder (SwinIA), the first convolution-free architecture for self-supervised denoising. It can be trained end-to-end with a simple mean squared error loss without masking and does not require any prior knowledge about clean data or noise distribution. Despite its simplicity, SwinIA establishes state-of-the-art on several common benchmarks.

1. Introduction

Image denoising aims to reconstruct true signal given corrupted input. The corruption depends on the camera sensor, signal processor, and other aspects of the image acquisition procedure, and can take various forms such as Gaussian noise, Poisson noise, salt-and-pepper noise, *etc.* Noise levels also vary with illumination and exposure, and some amount is always present in any image. This makes denoising an integral part of image processing pipelines.

Similar to other fields in computer vision, deep learning solutions [14, 2, 36, 34, 25, 18, 37, 33, 17, 24] have also superseded classical methods [4, 5, 22, 3] for denoising. However, when approached naively, neural networks require huge amounts of paired noisy and clean images for supervised learning. Collecting such a dataset is usually impracticable. Lehtinen *et al.* proposed Noise2Noise [17] and showed that supervision with independently corrupted data is equivalent to supervision with clean data. However, this approach still requires collecting multiple image copies, which may not be present in existing datasets.

Self-supervised denoising avoids the demand for paired data since it learns from the training dataset itself. Devel-



(a) Text token sequence. The representation of each token is built upon all other tokens, excluding the current one.

(b) Image pixel grid. Each pixel representation is derived from all other pixels, treating its own value as a blind spot.

Figure 1: Self-unaware autoencoding in text and images.

oping Noise2Noise ideas, Noisier2Noise [24] and Recorrupted2Recorrupted [25] applied additional noise on training images to emulate the strongly supervised Noise2Noise scenario. This was accomplished by assuming prior knowledge of the noise model. Self2Self [27] proposed training a network with Bernoulli input dropout and inference by ensembling outputs for several corrupted inputs. Neighbor2Neighbor [12] sub-sampled the input image and treated the result as independently corrupted copies for regularized training.

Noise2Self [2] and Noise2Void [14] introduced a different approach to self-supervised denoising — a blind-spot network (BSN). This type of network reconstructs a pixel from its neighborhood, assuming spatially independent zero-mean noise. It is practically difficult to dissect the continuous receptive field of convolutional neural networks (CNN), so BSNs usually use a masking procedure to hide a small portion of pixels by substitution [14] or random noise [2] and learn solely from them. However, learning from few data points per image slows down convergence, and different masking approaches may produce drastically different results [36]. Laine *et al.* [15] proposed to restrict the blindness by constructing four denoising branches with unidirectional receptive fields. In practice, this was achieved by passing four differently rotated input copies

through the network. Later, Honzàtko *et al.* [11] and Wu *et al.* [35] adopted dilated convolutions to create a true BSN which does not require masking. We further discuss these methods in Section 2. Subsequent works abandoned the idea of strict pixel blindness and adopted multiple forward passes through the network. Noise2Same [36] makes two forward passes (one with a random mask [2], one without) and regularizes the training with invariance loss in masked pixel locations. Blind2Unblind [34] utilizes global masking and combines the denoising result from passing five images through the network (four masked images with the gradient and one unmasked without).

Most recently, vision transformers started to outperform CNNs across a variety of benchmarks, including denoising. SwinIR [18], based on Swin Transformer [20], achieved state-of-the-art results in JPEG compression artifact reduction. Uformer [33] and Restormer [37] concurrently improved the results in camera noise removal. Evolution of vision transformers closely followed their path in natural language processing [8]. Bao *et al.* introduced BERT-style pre-training for image datasets [1], and He *et al.* showed that transformers are able to confidently reconstruct from the context up to 95% of hidden data in a masked autoencoder fashion [10]. These results hint that similar performance gains from flexibly accounting for long-range interactions could also benefit denoising models.

In this paper, we propose Swin Transformer-based Image Autoencoder (SwinIA), the first fully transformer-based architecture for self-supervised image denoising. SwinIA does not require any prior knowledge of noise distribution. It also does not have access to clean images, either through pre-training or knowledge distillation. Neither does it use input masking, auxiliary regularization losses, or multiple forward passes. Instead, SwinIA is trained as a plain autoencoder by minimizing the mean squared error (MSE) computed over the full image. We rigorously test our SwinIA method on a variety of synthetic and real-world datasets and demonstrate its competitiveness against state-of-the-art self-supervised denoising solutions.

2. Related work

We further describe the foundational ideas of blind spot networks and denoising vision transformers that our model is related to. We introduce their properties and usual training schemes and give the context for our advances.

2.1. Blind-spot networks

The blind-spot property is usually achieved by masking [14, 2, 16, 34] or multiple forward passes through the network [15, 34]. These techniques overcome the continuous receptive field issue of CNNs. It is also possible to maintain blindness with increasingly dilating convolutions. Honzàtko *et al.* [11] proposed a blind-spot convolutional

layer with a virtual “hole” in the kernel center. They designed an architecture with ten such layers in the decoder aggregating information from the respective levels of an encoder. This work followed the Laine *et al.* [15] training setup and demonstrated similar performance on sRGB datasets. The main limitation of this approach is the assumption that the noise distribution is known, and the network is merely tasked with estimating its parameters. Finally, Wu *et al.* [35] also utilized a dilated blind-spot network (DBSN) in a multi-stage pipeline with clean images provided via knowledge distillation.

2.2. Denoising vision transformers

Transformers are widely used for image restoration in the supervised setting [18, 33, 37], but rarely for self-supervised denoising. Zhang *et al.* proposed a Context-aware Denoise Transformer (CADT) [39] based on SwinIR [18] and Blind2Unblind [34] masking. They used Swin Transformer [20] blocks in the global branch of the network and trained them with patch embeddings, not pixel embeddings. However, they argued that a transformer alone is not suitable for the task and thus complemented it with convolutional local feature extraction. Liu *et al.* [19] built a single-image denoising transformer (DnT) from self-attention blocks interleaved with convolutional layers. This architecture was not tested for self-supervised denoising on large datasets.

3. Design

We were motivated by the performance of transformers on text and image data to develop them for a pure self-unaware denoising model.

3.1. Motivation

BSN was proposed many years ago [14, 2], but to date, no implementation strictly adhering to the original idea has been proposed. Existing solutions use masking [14, 2, 16, 34], assume known noise distributions [15, 11] or learn from clean data through knowledge distillation [35]. Thus, creating an assumption-free BSN that is trained end-to-end as an autoencoder remains an open challenge. As transformers learn comprehensive representations from unstructured data, we hypothesize that a variant of transformer architecture is suitable for this task.

3.2. Inspiration

3.2.1 Transformer-based image autoencoder

Shin *et al.* [31] introduced the idea of self-unaware text autoencoding using transformers (T-TA). They modified the transformer model so that each token representation is built based on all the other tokens, except itself, as in Figure 1a.

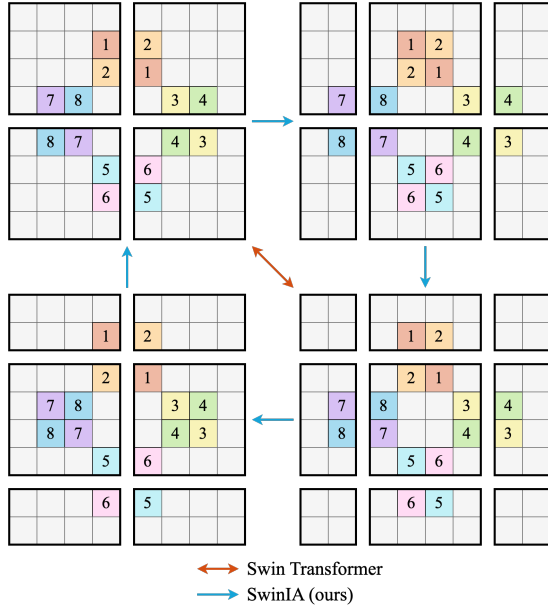


Figure 2: Shifted windows alternation between consequent transformer blocks. Neighboring pixel pairs that never occur in one window during the shifting flow of Swin Transformer [20] are enumerated 1 through 8.

T-TA builds text representations in one iteration without access to a token’s own value, as opposed to the masked language modeling objective of BERT [7], where the tokens are processed one at a time. We transfer this idea to the image domain to create a vision transformer autoencoder with self-unaware pixel-level tokens (Figure 1b).

3.2.2 Swin Transformer

In order to efficiently exploit a transformer-based model at the pixel level for high-dimensional image data, we need to use local attention. Swin Transformer [20] is a powerful multi-purpose vision model, which uses the (shifted) window multi-head self-attention ((S)W-MSA) mechanism that restricts self-attention to windows of fixed size. The windows are shifted from block to block to avoid bordering artifacts and spread the field of view [20].

Swin Transformer was already efficiently utilized at the pixel level in SwinIR [18], where individual pixels were embedded into transformer tokens.

3.3. Requirements

Combining the aforementioned ideas, we formulate a list of requirements that guided us in the design of a blind-spot transformer.

Self-unawareness. At any stage of the network, individual pixels should not have access to their own state on the previous levels. This is a primary feature of a blind-spot architecture that will prevent it from learning an identity function

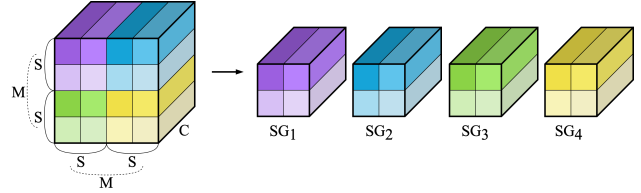


Figure 3: Window partition example with shuffle $S = 2$ into four shuffle groups. Window size is $M \times M = 2 \times 2$ shuffle groups, or 4×4 pixels.

through minimizing MSE loss.

Continuous field of view. Window transformers are widely used in image recognition tasks. However, they are usually rigid and therefore sometimes do not connect neighboring pixels. The usual diagonal window shift of Swin Transformer leads to some pixels never seeing their closest neighbors (Figure 2), and thus denoising artifacts. We need to design a solution where each pixel has a symmetrical and continuous receptive field.

Long-range interactions. Pooling layers downsample features and extract high-level information in the subsequent layers. However, in our setting, they disrupt input isolation by mixing together feature vectors of individual pixels. Therefore, we need a downsampling operation that enables attention between groups of pixels and at the same time, maintains the independence of each pixel.

U-shaped architecture. U-Net is arguably the most common blueprint for denoising networks. It operates in multiple scales and can pass information from encoder to decoder through skip connections. We need to design an architecture with similar properties holding to the assumptions listed above.

4. Methods

In this section, we describe the SwinIA model bottom-up, justifying the design choices according to the listed requirements referenced *in italics*.

4.1. Transformer block

The SwinIA transformer block (Figure 4) is based on Swin Transformer [20]. In contrast with pixel-level SwinIR [18], SwinIA operates at the level of **shuffle groups** — flattened square patches in the image of size $S \times S$ pixels. (S)W-MSA is computed between shuffle groups and is limited inside of a window of size $M \times M$ shuffle groups. An example of a window with partition into shuffle groups is presented in Figure 3. As a specific case, $S = 1$ means operating at the pixel level. Shuffle groups establish the demanded downsampling for *long-range interactions* and, thus, allow for a larger receptive field.

We follow the ideas from T-TA [31] in satisfying the requirement of *self-unawareness*. In (S)W-MSA, we mask the main diagonal of the attention matrix, so that the SoftMax

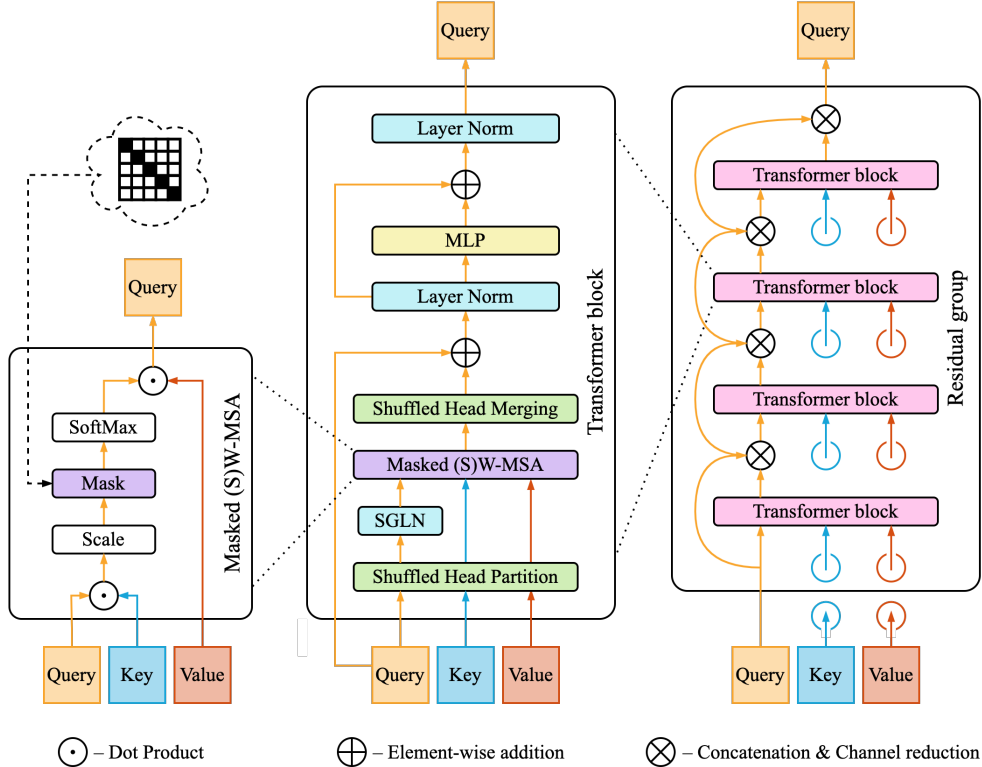


Figure 4: SwinIA residual group architecture. Circular portals \oplus and \otimes in the image represent inputting fixed Key and Value determined by input isolation.

values there become infinitesimal. Thus, none of the pixels attend to their own values. To maintain the blind-spot property throughout the transformer, we need to ensure input isolation. Thus, we need to keep keys and values separate from the transformed query. They solely act as inputs for (S)W-MSA to influence the output of the block.

As in Swin Transformer [20], there are two shortcuts by addition around (S)W-MSA and the multi-layer perceptron (MLP). Layer Normalization, however, is done after the shortcuts, as in the classical Transformer model for natural language [32]. We also propose Shuffle Group Layer Normalization (SGLN) for the query, in which each shuffle group is normalized for each attention head before (S)W-MSA.

4.2. Residual group

A residual group consists of 4 transformer blocks (see Figure 4). To achieve input isolation, queries are propagated through the blocks sequentially, while keys and values are fixed and passed into each transformer block unchanged. The query is skip-connected around each block via concatenation and linear projection back to the original embedding dimension.

As Swin Transformer [20] violates the *continuous field of view* requirement (Figure 2), we propose a cyclic shifting scheme, when the window is shifted to the right, bottom,

left, and back to the original in 4 consequent transformer blocks. An example demonstrating the difference between the two shifting schemes is given in Figure 2.

4.3. SwinIA model

The full SwinIA model architecture is presented in Figure 5. The model has a hierarchical *U-shaped structure*, where shuffle S changes from layer to layer.

Embedding. At the initial stage, the query is set to positional embeddings shared between all windows and attention heads. The input image is linearly projected separately into key and value and summed with the same positional embeddings. After this point, key and value stay unchanged and are passed as inputs into every residual group to maintain input isolation.

Encoder. The encoder consists of three residual groups with $S = 1, 2, 4$. The first group, therefore, works directly with pixels, and the other two expand their attention to a broader context. Around each group, there exists a skip connection that merges with the output by concatenation and projection, similarly to the shortcuts within a residual group. In contrast with U-Net [29], where the tensors are propagated down through the encoder, in SwinIA we cannot pass the output of a block with shuffle S_1 as an input for a block with shuffle S_2 if $S_1 < S_2$ without breaking the rule of *self-unawareness*. Otherwise, there would exist

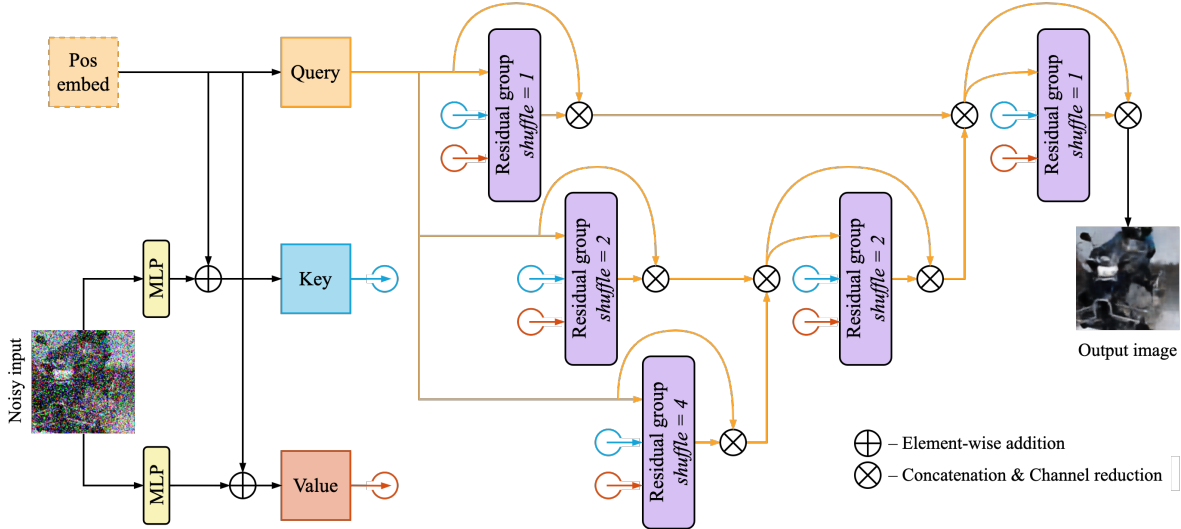


Figure 5: SwinIA model architecture. Circular portals \oplus and \otimes in the image represent inputting fixed Key and Value determined by input isolation.

mutual awareness between the elements of a single shuffle group coming from the previous layer. Thereby, each of the encoder shuffle groups takes identical inputs.

Decoder. The decoder consists of two shuffle groups symmetrical to those of the encoder, excluding the bottom one. In contrast with the encoder, we now can sequentially propagate tensors from group to group, as shuffles decrease by the decoder flow. As in the encoder, there are concatenation-and-projection skip connections around the shuffle groups. Apart from that, the outputs of the corresponding encoder groups are merged into inputs of the decoder blocks, in this, we follow the idea of global skip connections in U-Net [29].

5. Experimental results

We extensively test SwinIA against state-of-the-art self-supervised denoising methods on synthetic and real-world data. Since SwinIA is a true BSN and inevitably loses information from the masking, we separately focus on comparison with methods with similar properties [15, 35, 11]. We use the common metrics of peak signal-to-noise ratio (PSNR) and structural similarity index (SSIM) for evaluation. In addition to SwinIA, we implement and validate Noise2Self [2] and Noise2Same [36]. For the rest of the methods, we take the results from respective papers.

5.1. Training settings

We train SwinIA for 50 000 steps (unless mentioned otherwise) with batch size 64 and use Adam [13] with cosine annealing schedule [21] reducing learning rate from 10^{-3} to 10^{-6} . During training, we randomly crop 64×64 patches from images scaled to $[0, 1]$, rotate them by multiples of 90° , and flip them horizontally and vertically. Each patch

is standardized independently for $\mu = 0$ and $\sigma = 1$ except when synthetic Poisson noise is applied [36]. During validation, we pad each image for divisibility by 32 with reflection and crop the padding after prediction. We use 144 embeddings throughout the network, each transformer block has 16 heads, window size is set to 8.

We implemented all models in Python 3.8.3 and PyTorch 1.12.1 [26], and trained them on NVIDIA A100 80GB GPUs (driver version: 470.57.02, CUDA version: 11.4). We used `einops` [28] library for shuffling and tensor partitioning to attention heads and windows.

5.2. Synthetic noise (sRGB)

We follow [15, 12, 34] to create training and test sRGB datasets. For training, we select 44 328 images between 256×256 and 512×512 pixels from the ILSVRC2012 [6] validation set. For testing, we use Kodak [9], BSD300 [23], and Set14 [38], repeated by 10, 3, and 20 times, respectively. This adds up to 820 (240, 300, and 280) test images. We apply four types of noise in sRGB: (1) Gaussian noise with $\sigma = 25$, (2) Gaussian noise with $\sigma \in [5, 50]$, (3) Poisson noise with $\lambda = 30$, (4) Poisson noise with $\lambda \in [5, 50]$.

We present the results in Table 1. SwinIA performed similar to Noise2Void and Self2Self, however, did not improve over other true BSN methods. To our surprise, the method by Honzátka *et al.* [11] dominated the comparison despite being rarely mentioned in denoising literature.

5.3. Synthetic noise (grayscale)

Following [34], we use BSD400 [40] for training and test on Set12 and BSD68 [30] repeated 20 and 4 times, respectively. This results in 512 (240 and 272) testing images in total. We apply Gaussian noise with $\sigma = \{15, 25, 50\}$ to

Noise Type	Method	KODAK	BSD300	SET14
Gaussian $\sigma = 25$	Baseline, N2C [29]	32.43/0.884	31.05/0.879	31.40/0.869
	Baseline, N2N [17]	32.41/0.884	31.04/0.878	31.37/0.868
	CBM3D [4]	31.87/0.868	30.48/0.861	30.88/0.854
	Self2Self [27]	31.28/0.864	29.86/0.849	30.08/0.839
	N2V [14]	30.32/0.821	29.34/0.824	28.84/0.802
	Noisier2Noise [24]	30.70/0.845	29.32/0.833	29.64/0.832
	R2R [25]	32.25/0.880	30.91/0.872	<u>31.32/0.865</u>
	NBR2NBR [12]	32.08/0.879	30.79/0.873	31.09/0.864
	Blind2Undlind [34]	32.27/0.880	30.87/0.872	31.27/0.864
	Noise2Same [†] [36]	30.77/0.841	29.50/0.834	29.53/0.827
	Laine19-mu [15]	30.62/0.840	28.62/0.803	29.93/0.830
	Laine19-pme [15]	32.40/0.883	30.99/0.877	31.36/0.866
	DBSN [35]	31.64/0.856	29.80/0.839	30.63/0.846
	Honzatko20 [11]	32.45/-	31.02/-	31.25/-
Ours [†]	30.12/0.819	28.40/0.789	29.54/0.814	
Gaussian $\sigma \in [5, 50]$	Baseline, N2C [29]	32.51/0.875	31.07/0.866	31.41/0.863
	Baseline, N2N [17]	32.50/0.875	31.07/0.866	31.39/0.863
	CBM3D [4]	32.02/0.860	30.56/0.847	30.94/0.849
	Self2Self [27]	31.37/0.860	29.87/0.841	29.97/0.849
	N2V [14]	30.44/0.806	29.31/0.801	29.01/0.792
	R2R [25]	31.50/0.850	30.56/0.855	30.84/0.850
	NBR2NBR [12]	32.10/0.870	30.73/0.861	31.05/0.858
	Blind2Undlind [34]	32.34/0.872	30.86/0.863	31.14/0.857
	Noise2Same [†] [36]	30.78/0.835	29.49/0.823	29.34/0.817
	Laine19-mu [15]	30.52/0.833	28.43/0.794	29.71/0.822
	Laine19-pme [15]	32.40/0.870	30.95/0.861	<u>31.21/0.855</u>
	DBSN [35]	30.38/0.826	28.34/0.788	29.49/0.814
	Honzatko20 [11]	32.46/-	31.18/-	31.25/-
	Ours [†]	30.30/0.820	28.40/0.785	29.49/0.809
Poisson $\lambda = 30$	Baseline, N2C [29]	31.78/0.876	30.36/0.868	30.57/0.858
	Baseline, N2N [17]	31.77/0.876	30.35/0.868	30.56/0.857
	Anscombe [22]	30.53/0.856	29.18/0.842	29.44/0.837
	Self2Self [27]	30.31/0.857	28.93/0.840	28.84/0.839
	N2V [14]	28.90/0.788	28.46/0.798	27.73/0.774
	R2R [25]	30.50/0.801	29.47/0.811	29.53/0.801
	NBR2NBR [12]	31.44/0.870	30.10/0.863	30.29/0.853
	Blind2Undlind [34]	31.64/0.871	30.25/0.862	30.46/0.852
	Noise2Same [†] [36]	27.73/0.747	26.69/0.714	26.78/0.735
	Laine19-mu [15]	30.19/0.833	28.25/0.794	29.35/0.820
	Laine19-pme [15]	31.67/0.874	30.25/0.866	30.47/0.855
	DBSN [35]	30.07/0.827	28.19/0.790	29.16/0.814
	Honzatko20 [11]	31.67/-	30.25/-	30.14/-
	Ours [†]	29.51/0.805	27.92/0.775	28.74/0.799
Poisson $\lambda \in [5, 50]$	Baseline, N2C [29]	31.19/0.861	29.79/0.848	30.02/0.842
	Baseline, N2N [17]	31.18/0.861	29.78/0.848	30.02/0.842
	Anscombe [22]	29.40/0.836	28.22/0.815	28.51/0.817
	Self2Self [27]	29.06/0.834	28.15/0.817	28.83/0.841
	N2V [14]	28.78/0.758	27.92/0.766	27.43/0.745
	R2R [25]	29.14/0.732	28.68/0.771	28.77/0.765
	NBR2NBR [12]	30.86/0.855	29.54/0.843	29.79/0.838
	Blind2Undlind [34]	31.07/0.857	29.92/0.852	30.10/0.844
	Noise2Same [†] [36]	27.44/0.738	26.36/0.700	26.37/0.721
	Laine19-mu [15]	29.76/0.820	27.89/0.778	28.94/0.808
	Laine19-pme [15]	30.88/0.850	29.57/0.841	28.65/0.785
	DBSN [35]	29.60/0.811	27.81/0.771	28.72/0.800
	Ours [†]	29.06/0.788	27.74/0.764	28.27/0.780

Table 1: Denoising results on synthetic sRGB datasets. The highest PSNR(dB)/SSIM among unsupervised denoising methods is highlighted in **bold**, while the second-best is underlined. [†] denotes the models that we implemented and trained ourselves.

create noisy images.

The results are summarized in Table 2. Overall, our method performed on par with the existing solution. On

Noise Type	Method	Network	BSD68	Set12
Gaussian $\sigma = 15$	N2C [29]	U-Net [29]	31.58/0.889	32.60/0.899
	R2R [25]	U-Net [29]	31.54/0.885	32.54/0.897
	Noise2Self [†] [2]	U-Net [29]	30.63/0.843	29.88/0.840
	Noise2Same [†] [36]	U-Net [29]	30.85/0.850	30.02/0.849
	Blind2Unblind [34]	U-Net [29]	<u>31.44/0.884</u>	<u>32.46/0.897</u>
Ours	SwinIA	31.07/0.856	<u>30.37/0.857</u>	
Gaussian $\sigma = 25$	N2C [29]	U-Net [29]	29.02/0.822	30.07/0.852
	R2R [25]	U-Net [29]	28.99/0.818	<u>30.06/0.851</u>
	Noise2Self [†] [2]	U-Net [29]	28.88/0.789	28.37/0.799
	Noise2Same [†] [36]	U-Net [29]	<u>29.13/0.800</u>	28.54/0.814
	Blind2Unblind [34]	U-Net [29]	28.99/0.820	30.09/0.854
Ours	SwinIA	29.17/0.801	28.72/0.817	
Gaussian $\sigma = 50$	N2C [29]	U-Net [29]	26.08/0.715	26.88/0.777
	R2R [25]	U-Net [29]	26.02/0.705	<u>26.86/0.771</u>
	Noise2Self [†] [2]	U-Net [29]	26.19/0.664	25.56/0.692
	Noise2Same [†] [36]	U-Net [29]	26.75/0.714	26.13/0.744
	Blind2Unblind [34]	U-Net [29]	26.09/0.715	26.91/0.776
Ours [†]	SwinIA	<u>26.61/0.706</u>	26.03/0.736	

Table 2: Grayscale image denoising results for BSD68 and Set12 with synthetic noise. The highest PSNR(dB)/SSIM among unsupervised denoising methods is highlighted in **bold**, while the second-best is underlined. [†] denotes the models that we implemented and trained ourselves.

BSD68, in ranked first for $\sigma = 25$, second for $\sigma = 50$, and third for $\sigma = 15$. Interestingly, we obtained lower scores on Set12, but still consistently outperformed Noise2Self [2] as the only other method trained and inferred in a single forward pass.

5.4. Mixture synthetic noise

We experiment with the sRGB natural images dataset (ImageNet) and grayscale Chinese characters dataset (HànZi) with a mixture of multiple noise modalities, following [2, 36]. ImageNet dataset was generated by randomly cropping 60 000 patches of size 128×128 from the first 20 000 images in ILSVRC2012 [6] validation set that consists of 50 000 instances. We use two sets of 1 000 images for validation and testing. Poisson noise ($\lambda = 30$), additive Gaussian noise ($\sigma = 60$), and Bernoulli noise ($p = 0.2$) were applied to the clean images before the training.

HànZi dataset consists of 78 174 noisy images with 13 029 different Chinese characters of size 64×64 . Each noisy image is generated by applying Gaussian noise ($\sigma = 0.7$) and Bernoulli noise ($p = 0.5$) to a clean image. We select 10% of images for testing and use the rest for training.

We present the results in Table 3. On ImageNet, SwinIA outperformed the second-best method, Noise2Same [36], by +0.51dB PSNR and +0.013 SSIM. Compared to another true BSN by Laine *et al.* [15], SwinIA showed +2.47dB PSNR. On HànZi, SwinIA was worse than Noise2Same in PSNR (-0.5dB) but better in SSIM (+0.014). It also outperformed Laine *et al.* by +3.65dB PSNR. We compare example predictions with ground truth and noisy input in Figure 6 and 7.

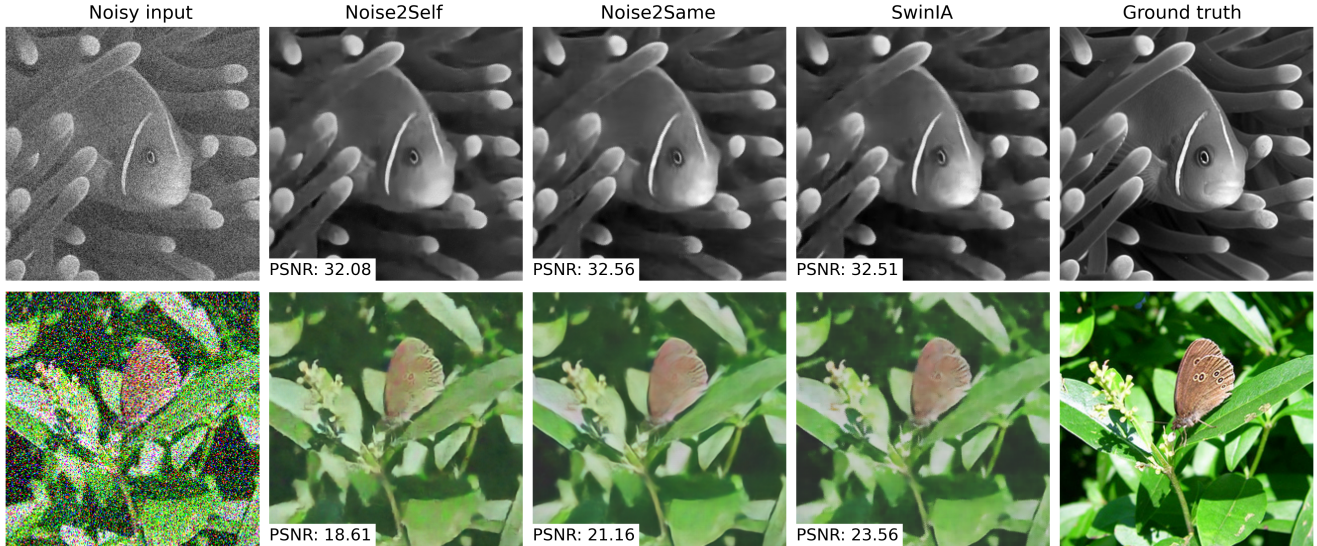


Figure 6: BSD68 [30] (top) and ImageNet [36] (bottom) denoising examples.

	ImageNet [0, 255] [36]	HànZi [0, 1] [2]
	Poisson $\lambda = 30$	
	Gaussian $\sigma \in [5, 50]$	Gaussian $\sigma = 0.7$
	Bernoulli $p = 0.2$	Bernoulli $p = 0.5$
Baseline, N2C [29]	23.39/-	15.66/-
Baseline, N2N [17]	23.27/-	14.30/-
NLM [3]	18.04/-	8.41/-
BM3D [5]	18.74/-	10.90/-
Noise2Void [14]	21.36/-	13.72/-
Noise2Self [†] [2]	21.33/0.574	14.16/0.512
Noise2Same [†] [36]	<u>22.85/0.625</u>	14.85/0.542
Laine19 [15]	20.89/-	10.70/-
Ours [†]	23.36/0.638	<u>14.35/0.556</u>

Table 3: Denoising results on synthetic datasets in sRGB space with mixed noise [36]. The highest PSNR(dB)/SSIM among unsupervised denoising methods is highlighted in **bold**, while the second-best is underlined. [†] denotes the models that we implemented and trained ourselves.

5.5. Fluorescent microscopy

We use Confocal Fish, Confocal Mice, and Two-Photon Mice datasets from the Fluorescent Microscopy Denoising Dataset [41]. Each dataset consists of 20 views, with 50 grayscale images per view. Each image contains a mixture of natural Poisson and Gaussian noise. Ground truth image for the view is obtained by averaging all images. We follow [34] and select the 19th view for testing and the rest for training. To avoid overfitting, we set the number of steps to 20 000 and apply weight decay 10^{-8} .

Experimental results are presented in Table 4. SwinIA performed competitively across all datasets. Another true BSN method by Laine *et al.* [15] required knowledge about the noise model and performed worse for the real-world microscopy data with noise mixture: on average, SwinIA was better by 0.2db PSNR and 0.01 SSIM than Laine19-mu for

Methods	Network	Confocal Fish	Confocal Mice	Two-Photon Mice
Baseline, N2C [29]	U-Net [29]	32.79/0.905	38.40/0.966	34.02/0.925
Baseline, N2N [17]	U-Net [29]	32.75/0.903	38.37/0.965	33.80/0.923
BM3D [5]	-	32.16/0.886	37.93/0.963	33.83/0.924
N2V [14]	U-Net [29]	32.08/0.886	37.49/0.960	33.38/0.916
NBR2NBR [12]	U-Net [29]	32.11/0.890	37.07/0.960	33.40/0.921
Blind2Undlind [34]	U-Net [29]	32.74/0.897	38.44/0.964	34.03/0.916
Noise2Self [†] [2]	U-Net [29]	31.96/0.877	36.45/0.960	31.61/0.910
Noise2Same [†] [36]	U-Net [29]	32.36/0.893	37.64/0.960	33.55/0.917
Denoise Transformer[39]	CADT[39]	<u>32.52/0.895</u>	<u>38.21/0.962</u>	33.64/0.914
Laine19-mu (G) [15]	U-Net [29]	31.62/0.849	37.54/0.959	32.91/0.903
Laine19-pme (G) [15]	U-Net [29]	23.30/0.527	31.64/0.881	25.87/0.418
Laine19-mu (P) [15]	U-Net [29]	31.59/0.854	37.30/0.956	33.09/0.907
Laine19-pme (P) [15]	U-Net [29]	25.16/0.597	37.82/0.959	31.80/0.820
Ours [†]	SwinIA	31.79/0.871	37.65/0.960	33.25/0.915

Table 4: Denoising results on Fluorescent Microscopy datasets. The highest PSNR(dB)/SSIM among unsupervised denoising methods is highlighted in **bold**, while the second-best is underlined. For Laine *et al.* [15], G stands for Gaussian, P is for Poisson. [†] denotes the models that we implemented and trained ourselves.

both Gaussian and Poisson assumed distributions.

5.6. Ablation study

We ran ablation experiments on mixed noise sRGB ImageNet dataset to validate architecture design elements proposed in Sections 3.3 and 4 as well as additional hyperparameters. The results are summarized in Table 5. In particular, we found that the original Swin Transformer [20] diagonal shift leads to a substantial performance decrease and visible tiling artifacts. Shuffle GroupNorm slightly improves the results, and Cosine Annealing learning rate schedule [21] leads to a better convergence compared to decreasing learning rate by half every 5 000 steps [36]. When we removed the U-shaped shuffle configuration and naively

stacked transformer blocks without shuffle, training did not converge at all.

	Diagonal shift [20]	Cyclic shift	Lambda LR [36]	Cosine LR [21]	Shuffle Group LN	U-Shuffle	PSNR/SSIM	Δ
Our best		✓		✓	✓	✓	23.36/0.638	
Ablation	No Cyclic shift	✓		✓	✓	✓	23.10/0.623	-0.26/-0.015
	No Cosine LR		✓	✓	✓	✓	23.16/0.627	-0.20/-0.011
	No SGLN		✓	✓	✓	✓	23.30/0.631	-0.06/-0.007
	No U-Shuffle		✓	✓	✓	✓	—	

Table 5: Ablation results on ImageNet dataset with mixed noise [36].

We also checked the necessity of shortcuts around transformer blocks and the last Layer Normalization in the block. The results of this ablation on Hànzì and ImageNet are summarized in Table 6. Removing any of the components had a mixed effect on the performance. For example, without the last Layer Normalization, performance on ImageNet slightly improved, however, it drastically dropped for Hànzì. The opposite was true for the shortcuts: excluding them provided slightly better results for Hànzì, but considerably weakened the scores on ImageNet. For our final architecture, we chose the most balanced solution and included both elements.

	Hànzì [2]	ImageNet [36]
Our best	<u>14.35/0.556</u>	<u>23.36/0.638</u>
No shortcuts	14.36/0.559	23.24/0.624
No last norm	13.91/0.543	23.40/0.638

Table 6: Ablation results for transformer group architecture details on Hànzì [2] and ImageNet [36].

6. Discussion

We designed our SwinIA model to be flexible and robust in various noise conditions. It showed state-of-the-art results on ImageNet with a mixture of Gaussian, Poisson, and Bernoulli noise. It also performed better than other true blind-spot methods on a fluorescent microscopy dataset with natural noise. Among datasets with single-distribution synthetic noise, SwinIA performed best for BSD68 across multiple σ of Gaussian. However, it did not match the best methods on other test datasets, performing on par with Noise2Void [14], DBSN [35], and Self2Self [27]. We hypothesize that this is due to the inherent limitations of blind-spot models. The pixel itself contains the most useful information about its true signal, which is inevitably lost in the training process. However, this gives substantial room for improvement in our method. Different masking strategies

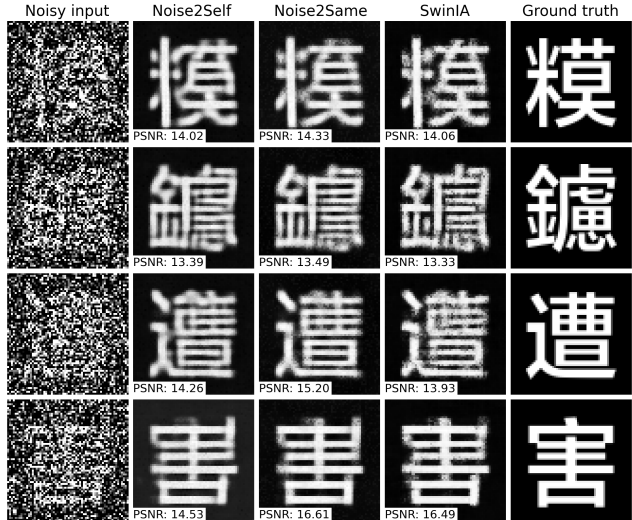


Figure 7: Denoising results on Hànzì [2] images.

and regularization techniques were proposed to loosen the blindness requirement [34, 36]. Similar approaches could be applicable to the diagonal attention mask as well.

From the blind-spot property comes the second limitation of our model. Similarly to other BSNs, it assumes spatially uncorrelated noise. For many digital photography datasets with natural noise, this is not the case because of hardware pixel interpolation. We hypothesize that correlated noise can be mitigated with increased shuffle group size resembling the approach by Lee *et al.* [16] if the correlation is present only in a close neighborhood.

Finally, transformers are considerably more computationally expensive than the usual denoising U-Net and require more time for training and inference. However, they are known for their ability to extract meaningful representations from large datasets, and we expect our method to improve with increasing training set size. Besides, being conceptually similar to the language modeling objective [31], our solution could be used in self-supervised pre-training to produce rich pixel embeddings for downstream image processing tasks.

7. Conclusion

We propose a Swin Transformer-based Image Autoencoder, the first convolution-free transformer architecture for blind-spot self-supervised denoising. Unlike its counterparts, it does not assume any knowledge about noise distribution. It also does not use masking and can be trained in an autoencoder fashion with a single forward pass and an MSE loss. Despite the loss of information from the blind spot and ignorance of the noise nature, it achieves competitive results, outperforming state-of-the-art denoising methods on several datasets.

References

- [1] Hangbo Bao, Li Dong, Songhao Piao, and Furu Wei. Beit: Bert pre-training of image transformers. *arXiv preprint arXiv:2106.08254*, 2021. **2**
- [2] Joshua Batson and Loic Royer. Noise2Self: Blind denoising by self-supervision. In Kamalika Chaudhuri and Ruslan Salakhutdinov, editors, *Proceedings of the 36th International Conference on Machine Learning*, volume 97 of *Proceedings of Machine Learning Research*, pages 524–533. PMLR, 09–15 Jun 2019. **1, 2, 5, 6, 7, 8, 11, 12, 13, 14, 15**
- [3] Antoni Buades, Bartomeu Coll, and J-M Morel. A non-local algorithm for image denoising. In *2005 IEEE computer society conference on computer vision and pattern recognition (CVPR'05)*, volume 2, pages 60–65. Ieee, 2005. **1, 7**
- [4] Kostadin Dabov, Alessandro Foi, Vladimir Katkovnik, and Karen Egiazarian. Color image denoising via sparse 3d collaborative filtering with grouping constraint in luminance-chrominance space. volume 1, pages I – 313, 09 2007. **1, 6**
- [5] Kostadin Dabov, Alessandro Foi, Vladimir Katkovnik, and Karen Egiazarian. Image denoising by sparse 3-d transform-domain collaborative filtering. *IEEE Transactions on image processing*, 16(8):2080–2095, 2007. **1, 7**
- [6] Jia Deng, Wei Dong, Richard Socher, Li-Jia Li, Kai Li, and Li Fei-Fei. Imagenet: A large-scale hierarchical image database. In *CVPR*, pages 248–255, 2009. **5, 6, 11**
- [7] Jacob Devlin, Ming-Wei Chang, Kenton Lee, and Kristina Toutanova. BERT: Pre-training of deep bidirectional transformers for language understanding. In *Proceedings of the 2019 Conference of the North American Chapter of the Association for Computational Linguistics: Human Language Technologies, Volume 1 (Long and Short Papers)*, pages 4171–4186, Minneapolis, Minnesota, June 2019. Association for Computational Linguistics. **3**
- [8] Alexey Dosovitskiy, Lucas Beyer, Alexander Kolesnikov, Dirk Weissenborn, Xiaohua Zhai, Thomas Unterthiner, Mostafa Dehghani, Matthias Minderer, Georg Heigold, Sylvain Gelly, et al. An image is worth 16x16 words: Transformers for image recognition at scale. *arXiv preprint arXiv:2010.11929*, 2020. **2**
- [9] Rich Franzen. Kodak lossless true color image suite. source: <http://r0k.us/graphics/kodak>, 4(2), 1999. **5, 12**
- [10] Kaiming He, Xinlei Chen, Saining Xie, Yanghao Li, Piotr Dollár, and Ross Girshick. Masked autoencoders are scalable vision learners. In *Proceedings of the IEEE/CVF Conference on Computer Vision and Pattern Recognition*, pages 16000–16009, 2022. **2**
- [11] David Honzátko, Siavash A Bigdeli, Engin Türetken, and L Andrea Dunbar. Efficient blind-spot neural network architecture for image denoising. In *2020 7th Swiss Conference on Data Science (SDS)*, pages 59–60. IEEE, 2020. **2, 5, 6**
- [12] Tao Huang, Songjiang Li, Xu Jia, Huchuan Lu, and Jianzhuang Liu. Neighbor2neighbor: Self-supervised denoising from single noisy images. In *Proceedings of the IEEE/CVF conference on computer vision and pattern recognition*, pages 14781–14790, 2021. **1, 5, 6, 7, 12**
- [13] Diederik P Kingma and Jimmy Ba. Adam: A method for stochastic optimization. *arXiv preprint arXiv:1412.6980*, 2014. **5**
- [14] Alexander Krull, Tim-Oliver Buchholz, and Florian Jug. Noise2void-learning denoising from single noisy images. In *Proceedings of the IEEE/CVF Conference on Computer Vision and Pattern Recognition*, pages 2129–2137, 2019. **1, 2, 6, 7, 8**
- [15] Samuli Laine, Tero Karras, Jaakko Lehtinen, and Timo Aila. High-quality self-supervised deep image denoising. *Advances in Neural Information Processing Systems*, 32, 2019. **1, 2, 5, 6, 7, 12**
- [16] Wooseok Lee, Sanghyun Son, and Kyoung Mu Lee. Apbsn: Self-supervised denoising for real-world images via asymmetric pd and blind-spot network. In *Proceedings of the IEEE/CVF Conference on Computer Vision and Pattern Recognition*, pages 17725–17734, 2022. **2, 8**
- [17] Jaakko Lehtinen, Jacob Munkberg, Jon Hasselgren, Samuli Laine, Tero Karras, Miika Aittala, and Timo Aila. Noise2noise: Learning image restoration without clean data. *arXiv preprint arXiv:1803.04189*, 2018. **1, 6, 7**
- [18] Jingyun Liang, Jie Zhang Cao, Guolei Sun, Kai Zhang, Luc Van Gool, and Radu Timofte. Swinir: Image restoration using swin transformer. *arXiv preprint arXiv:2108.10257*, 2021. **1, 2, 3**
- [19] Xiaolong Liu, Yusheng Hong, Qifang Yin, and Shuo Zhang. Dnt: Learning unsupervised denoising transformer from single noisy image. In *Proceedings of the 4th International Conference on Image Processing and Machine Vision, IPMV '22*, page 50–56, New York, NY, USA, 2022. Association for Computing Machinery. **2**
- [20] Ze Liu, Yutong Lin, Yue Cao, Han Hu, Yixuan Wei, Zheng Zhang, Stephen Lin, and Baining Guo. Swin transformer: Hierarchical vision transformer using shifted windows. In *Proceedings of the IEEE/CVF International Conference on Computer Vision (ICCV)*, 2021. **2, 3, 4, 7, 8**
- [21] Ilya Loshchilov and Frank Hutter. Sgdr: Stochastic gradient descent with warm restarts. *arXiv preprint arXiv:1608.03983*, 2016. **5, 7, 8**
- [22] Markku Makitalo and Alessandro Foi. Optimal inversion of the anscombe transformation in low-count poisson image denoising. *IEEE Transactions on Image Processing*, 20(1):99–109, 2011. **1, 6**
- [23] David Martin, Charless Fowlkes, Doron Tal, and Jitendra Malik. A database of human segmented natural images and its application to evaluating segmentation algorithms and measuring ecological statistics. In *ICCV*, volume 2, pages 416–423, 2001. **5, 12**
- [24] Nick Moran, Dan Schmidt, Yu Zhong, and Patrick Coady. Noisier2noise: Learning to denoise from unpaired noisy data. In *Proceedings of the IEEE/CVF Conference on Computer Vision and Pattern Recognition*, pages 12064–12072, 2020. **1, 6**
- [25] Tongyao Pang, Huan Zheng, Yuhui Quan, and Hui Ji. Recorrupted-to-recorrupted: unsupervised deep learning for image denoising. In *Proceedings of the IEEE/CVF conference on computer vision and pattern recognition*, pages 2043–2052, 2021. **1, 6**

- [26] Adam Paszke, Sam Gross, Soumith Chintala, Gregory Chanan, Edward Yang, Zachary DeVito, Zeming Lin, Alban Desmaison, Luca Antiga, and Adam Lerer. Automatic differentiation in pytorch. 2017. [5](#), [11](#)
- [27] Yuhui Quan, Mingqin Chen, Tongyao Pang, and Hui Ji. Self2self with dropout: Learning self-supervised denoising from single image. In *Proceedings of the IEEE/CVF conference on computer vision and pattern recognition*, pages 1890–1898, 2020. [1](#), [6](#), [8](#)
- [28] Alex Rogozhnikov. Einops: Clear and reliable tensor manipulations with einstein-like notation. In *International Conference on Learning Representations*, 2022. [5](#), [11](#)
- [29] Olaf Ronneberger, Philipp Fischer, and Thomas Brox. U-net: Convolutional networks for biomedical image segmentation. In Nassir Navab, Joachim Hornegger, William M. Wells, and Alejandro F. Frangi, editors, *Medical Image Computing and Computer-Assisted Intervention – MICCAI 2015*, pages 234–241, Cham, 2015. Springer International Publishing. [4](#), [5](#), [6](#), [7](#)
- [30] Stefan Roth and Michael J Black. Fields of experts: A framework for learning image priors. In *CVPR*, pages 860–867. IEEE, 2005. [5](#), [7](#), [12](#)
- [31] Joongbo Shin, Yoonhyung Lee, Seunghyun Yoon, and Kyomin Jung. Fast and accurate deep bidirectional language representations for unsupervised learning. In *Proceedings of the 58th Annual Meeting of the Association for Computational Linguistics*, pages 823–835, Online, July 2020. Association for Computational Linguistics. [2](#), [3](#), [8](#)
- [32] Ashish Vaswani, Noam Shazeer, Niki Parmar, Jakob Uszkoreit, Llion Jones, Aidan N Gomez, Łukasz Kaiser, and Illia Polosukhin. Attention is all you need. In I. Guyon, U. Von Luxburg, S. Bengio, H. Wallach, R. Fergus, S. Vishwanathan, and R. Garnett, editors, *Advances in Neural Information Processing Systems*, volume 30. Curran Associates, Inc., 2017. [4](#)
- [33] Zhendong Wang, Xiaodong Cun, Jianmin Bao, Wengang Zhou, Jianzhuang Liu, and Houqiang Li. Uformer: A general u-shaped transformer for image restoration. In *Proceedings of the IEEE/CVF Conference on Computer Vision and Pattern Recognition*, pages 17683–17693, 2022. [1](#), [2](#)
- [34] Zejin Wang, Jiazheng Liu, Guoqing Li, and Hua Han. Blind2unblind: Self-supervised image denoising with visible blind spots. In *Proceedings of the IEEE/CVF Conference on Computer Vision and Pattern Recognition*, pages 2027–2036, 2022. [1](#), [2](#), [5](#), [6](#), [7](#), [8](#), [12](#), [14](#), [15](#)
- [35] Xiaohe Wu, Ming Liu, Yue Cao, Dongwei Ren, and Wangmeng Zuo. Unpaired learning of deep image denoising. In *Computer Vision—ECCV 2020: 16th European Conference, Glasgow, UK, August 23–28, 2020, Proceedings, Part IV*, pages 352–368. Springer, 2020. [2](#), [5](#), [6](#), [8](#)
- [36] Yaochen Xie, Zhengyang Wang, and Shuiwang Ji. Noise2Same: Optimizing a self-supervised bound for image denoising. In *Advances in Neural Information Processing Systems*, volume 33, pages 20320–20330, 2020. [1](#), [2](#), [5](#), [6](#), [7](#), [8](#), [11](#), [12](#), [13](#), [14](#), [15](#)
- [37] Syed Waqas Zamir, Aditya Arora, Salman Khan, Munawar Hayat, Fahad Shahbaz Khan, and Ming-Hsuan Yang. Restormer: Efficient transformer for high-resolution image restoration. In *Proceedings of the IEEE/CVF Conference on Computer Vision and Pattern Recognition*, pages 5728–5739, 2022. [1](#), [2](#)
- [38] Roman Zeyde, Michael Elad, and Matan Protter. On single image scale-up using sparse-representations. In *International conference on curves and surfaces*, pages 711–730, 2010. [5](#), [12](#)
- [39] Dan Zhang and Fangfang Zhou. Self-supervised image denoising for real-world images with context-aware transformer. *IEEE Access*, 2023. [2](#), [7](#)
- [40] Kai Zhang, Wangmeng Zuo, Yunjin Chen, Deyu Meng, and Lei Zhang. Beyond a gaussian denoiser: Residual learning of deep cnn for image denoising. *TIP*, 26(7):3142–3155, 2017. [5](#), [11](#)
- [41] Yide Zhang, Yin hao Zhu, Evan Nichols, Qingfei Wang, Siyuan Zhang, Cody Smith, and Scott Howard. A poisson-gaussian denoising dataset with real fluorescence microscopy images. In *CVPR*, 2019. [7](#), [11](#), [12](#), [16](#)

A. Model card

Table 7: Model Card of SwinIA model.

Model Summary	
Model Architecture	Fully transformer-based image autoencoder model for end-to-end self-supervised image denoising with no convolutions. For details, see Section 4.
Input(s)	The model takes noisy images as input, batch and channel dimensions go first.
Output(s)	The model outputs a batch of denoised images of the same shape as input.
Usage	
Application	The model can be used in self-supervised image denoising for any type of spatially-uncorrelated synthetic and natural noise on both grayscale and colored images. Also, it is theoretically possible to use the model in self-supervised pre-training for extracting features from images for downstream computer vision tasks.
Known Limitations	The model is computationally expensive and requires both powerful GPU hardware and considerable training time. Also, small datasets will most probably lead to overfitting. Finally, the model will most likely learn an identity function on the data with spatially correlated noise without proper tuning of shuffle group sizes (as discussed in Section 6).
System Type	
System Description	This is a standalone model.
Upstream Dependencies	None.
Downstream Dependencies	None.
Implementation Frameworks	
Hardware & Software	Hardware: NVIDIA A100 80GB GPUs (driver version: 470.57.02, CUDA version: 11.4). Software: Python 3.8.3, PyTorch 1.12.1 [26], einops [28].
Compute Requirements	SwinIA was trained on 2 NVIDIA A100 80GB GPUs for different numbers of steps (see Section 5 for details).
Model Characteristics	
Model Initialization	The model is trained from a random initialization.
Model Status	This is a static model trained on offline datasets.
Model Stats	SwinIA model has 2.369 million parameters and performs 10.117 GFLOPS (floating point operations per second) for a single grayscale image of size 64×64 .
Data Overview	
Training Datasets	Synthetic noise (sRGB): ILSVRC2012 [6] validation set (Section 5.2). Synthetic noise (grayscale): BSD400 [40] (Section 5.3). Mixture synthetic noise: ImageNet [36], Hànzì [2, 36] (Section 5.4). Natural noise (grayscale): Confocal Fish, Confocal Mice, and Two-Photon Mice datasets from the Fluorescent Microscopy Denoising Dataset [41] (Section 5.5).

Evaluation Datasets	Synthetic noise (sRGB): Kodak [9], BSD300 [23], Set14 [38] (Section 5.2).
	Synthetic noise (grayscale): Set12 and BSD68 [30] (Section 5.3).
	Mixture synthetic noise: ImageNet [36], HânZì [2, 36] (Section 5.4).
	Natural noise (grayscale): Confocal Fish, Confocal Mice, and Two-Photon Mice datasets from the Fluorescent Microscopy Denoising Dataset [41] (Section 5.5).

Dataset	Noise2Same		SwinIA	
	TT (h)	AIT (ms)	TT (h)	AIT (ms)
Synthetic (sRGB) [15, 12, 34]	4	26	15	941
Synthetic (grayscale) [34]	2	12	13	605
ImageNet [36]	1	14	15	765
HânZì [2]	1	5	14	42
Microscopy [15, 12, 34]	1.5	20	5	845

Table 8: Comparison of training time (TT) in hours, and average inference time (AIT) on the test set in milliseconds of Noise2Same [36] and SwinIA (ours) on various datasets.

Criterion	Noise2Same	SwinIA
Number of trainable parameters	5.564M	2.369M
FLOPs per grayscale image 64×64	5.001G	10.117G

Table 9: Comparison of the number of parameters and FLOPS between Noise2Same [36] and SwinIA (ours). The number of FLOPS is calculated for inference time, as Noise2Same has two forward passes during training, and this number gets doubled.

B. Model complexity

We compare the training time and average inference time of Noise2Same [36] and SwinIA models in Table 8 and show the difference in the number of parameters and the number of floating point operations per second (FLOPS) in Table 9.

C. Failed experiments

We tried a multitude of configurations and training schemes, and not all of them were successful. Here, we list some approaches that we found interesting but did not manage to train properly.

Noise2Same training. We have tried to train SwinIA in Noise2Same [36] mode with two forward passes. In the first, masked, pass we applied diagonal masking as in the baseline. In the second pass, we did not mask the attention, allowing each pixel to look at itself. We also lifted

the input isolation requirement and computed self-attention starting from the second transformer block. Thus, we obtained two outputs and measured invariance loss (RMSE) between them and MSE between the masked output and the input. In this configuration, training did not converge well. We assume that the network is confused about the modality shift between the two passes.

Dilated attention. Instead of pixel shuffle, we tested dilated window attention as a way to improve the receptive field. However, such a model resulted in rigid pixel-level artifacts due to the attention sparsity that went against the importance of dense pixel interactions.

D. Denoising results visualization

In Figures 8, 9, 10, and 11, we present additional examples from several experiments and discuss details in figure captions.



Figure 8: Denoising examples on ImageNet dataset with mixed synthetic noise [36]. Each row contains noisy and ground truth images, along with the predictions of Noise2Self [2], Noise2Same [36], and SwinIA (ours) models with corresponding PSNR scores. Each image is center-cropped for visualization. SwinIA appears to be more capable of restoring random detailed structures (as in the image with tree bark and the corals) and does not tend to excessively smooth the background.



Figure 9: Denoising examples on BSD68 dataset with synthetic Gaussian noise with $\sigma = 25$ [34]. Each row contains noisy and ground truth images, along with the predictions of Noise2Self [2], Noise2Same [36], and SwinIA (ours) models with corresponding PSNR scores. Each image is center-cropped for visualization. SwinIA shows competitive performance, achieving slightly better scores in most cases.



Figure 10: Denoising examples on Set12 dataset with synthetic Gaussian noise with $\sigma = 25$ [34]. Each row contains noisy and ground truth images, along with the predictions of Noise2Self [2], Noise2Same [36], and SwinIA (ours) models with corresponding PSNR scores. Each image is center-cropped for visualization. In the image with striped clothes (third row), SwinIA outperforms its counterparts in the restoration of clothing patterns.

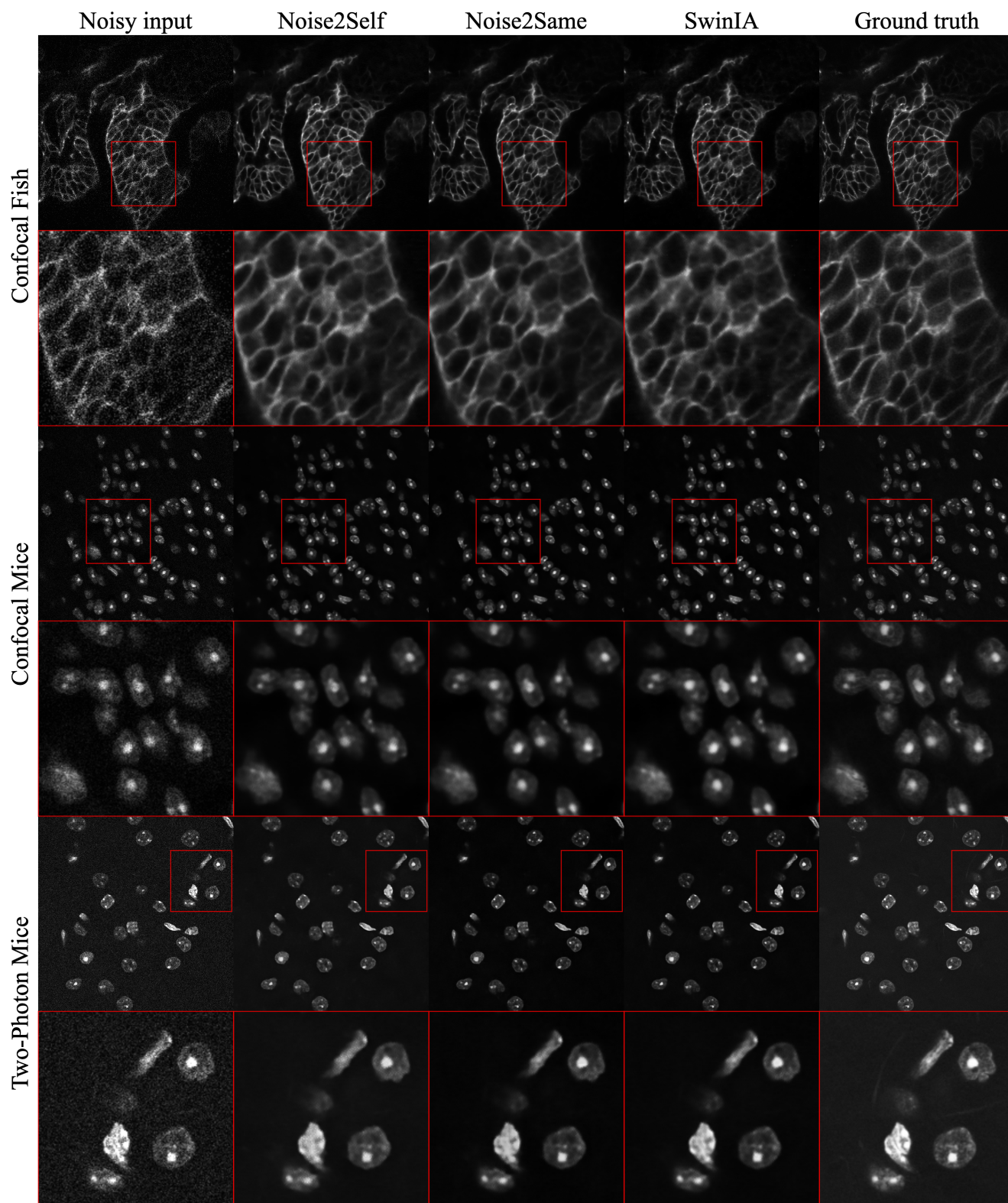


Figure 11: Denoising results on fluorescent microscopy images with natural noise [41]. Each pair of rows shows an example from each of the three used datasets, zooming a partition of each image for a better view.